Article Type: Original Paper

Title: Non-Paraxial Polarization Spatio-Temporal Coupling in Ultrafast Laser Material Processing

Aabid Patel[1], Vladmir T. Tikhonchuk[2], Jingyu Zhang[1] and Peter G. Kazansky[1]*

*Corresponding Author: ap7g12@orc.soton.ac.uk

[1]Optoelectronics Research Centre, University of Southampton, SO17 1BJ, United Kingdom
[2]University of Bordeaux – CNRS - CEA, CELIA, UMR 5107, 33405 Talence, France

Abstract

Two hundred years after Malus' discovery of optical anisotropy, the study of polarization-driven optical effects is as active as ever, generating interest in new phenomena and potential applications. However, in ultrafast optics, the influence of polarization is frequently overlooked being considered as either detrimental or negligible. Here we demonstrate that spatio-temporal couplings, which are inherent for ultrafast laser systems with chirped-pulse amplification, accumulate in multi-pulse irradiation and lead to a strongly anisotropic light-matter interaction. Our results identify angular dispersion in the focus as the origin for the polarization dependence in modification, yielding an increase in modification strength. With tight focusing (NA ≥ ~0.4), this non-paraxial effect leads to a manifestation of spatio-temporal couplings in photo-induced modification. We devise a practical way to control the polarization dependence and exploit it as a new degree of freedom in tailoring laser-induced modification in transparent material. A near-focus, non-paraxial field structure analysis of an optical beam provides insight on the origin of the polarization dependent modification. However, single pulse non-paraxial corrected calculations are not sufficient to explain the phenomena confirming the experimental observations and exemplifying the need for multi-pulse analysis.

1. Introduction

Broad spectrum is one of the key requirements for ultrafast laser systems. The invention of effective mechanisms capable of locking spectral components in phase paved the way towards pulses as short as several femtoseconds. Given that these ultrashort pulses have durations near the timescales of fundamental molecular and atomic processes, they have found a wide variety of applications stretching from observing photochemical processes on femtosecond time scales[1], to selectively instigating molecular excitation via adaptive quantum control.[2] Nonlinear processes triggered by ultrafast laser pulses have revolutionized the world of microscopy through targeted nonlinear excitation techniques. In particular, second- and third-harmonic generation microscopy as well as multiphoton microscopy provide the best non-invasive means for biological imaging.[3] Femtosecond lasers have also been successfully applied to non-invasive surgeries in the bulk of human tissue with sub-micrometer resolution without collateral damage.[4] This comes at the price of taking extra care to control phase of the pulse, which can be disturbed by dispersive media or self-phase modulation, and lead to a significant decrease of pulse intensity. Normally, this is seen as a negative effect. However, a method called chirped-pulse amplification (*CPA)* clearly demonstrated that the manipulation of spectral components could be exploited for the benefit by providing a manner of alleviating the issue of damaging the gain medium by excessive intensities by temporarily stretching out a pulse before the gain medium. The amplified pulse is then recompressed back to the original pulse width in the same manner it was stretched by, enabling terawatt to petawatt intensities.[5,6] Recently, simultaneous spatial and temporal focusing (*SSTF*) has shown promise in overcoming nonlinear side-effects when reaching the critical power near the focus, not only in material modification[7–12], but also in microscopy and tissue ablation[13–16] and atmospheric propagation.[17] This is accomplished by separating the spatial components of the incident light pulse. Each portion of the beam then carries a reduced local-bandwidth, resulting

in an increased overall pulse duration and reduced intensity. Upon focusing, the separated components are brought back together recovering the initial bandwidth and duration of the laser pulse. As a result, the maximum light intensity is only observed near the focus. Thus, nonlinear phenomena are localized at the focus as opposed to conventional focusing of a transform limited femtosecond-picosecond laser pulse.

Normally working with temporal and spatial dependences like those seen within SSTF and CPA, the vectorial nature of the spatio-temporal couplings is overlooked. Spatial chirp (spread of frequency components across the beam front; *SC*)[18], pulse front tilt (inclination of the intensity front with respect to the propagation direction; *PFT*)[19], angular dispersion (angular separation of light rays of differing frequencies; *AD*)[20,21] and wavefront rotation/Time vs. Angle (rotation of wavefront in time - lighthouse effect*; WFR/TVA*)[22,23] have all been discussed individually from a theoretical point of view and thorough experimental techniques have been developed to characterize them.[24] Previous studies have clearly indicated that spatio-temporal couplings can give rise to strong directional dependence and more importantly anisotropic photosensitivity in isotropic homogeneous materials[25–29], which is thought to depend on the polarization orientation with respect to the azimuth of the PFT and is known as the *blade effect.*[25] With no effective control of the vectorial dependences, the benefits of the phenomenon cannot be exploited. As a result, this polarization dependent behavior is normally seen as detrimental for applications where precision of the process is essential. Here we demonstrate that spatial and temporal components can be separately controlled with the use of an external grating pair, in conjunction with the stretcher/compressor system built into the CPA set-up, allowing us to investigate spatio-temporal dependences on ultrafast laser induced material modification. With this, we demonstrate that this observed polarization dependence in modification is an inherent property in the interaction of transparent media in the femtosecond domain and it can be observed in a range of materials. Analysis of the linear behavior of spatio-

temporal couplings in and out of the focus using linear propagation simulations allows us to understand how different potential mechanisms evolve in the focal volume. From here, the spatio-temporal coupling, which plays a dominant role in the polarization dependent modification, is determined.

2. Spatio-Temporal Couplings

In ultrafast laser systems, PFT can easily occur because of CPA, where the pulse is stretched before entering an amplifier. Although the pulse is afterwards compressed, the residual spatio-temporal couplings can still be present. AD will cause the different frequency components of the laser pulse to propagate at different angles. As a result, the beam would expand in the direction of the dispersion upon propagation yielding a constantly expanding elliptical shape. Whereas, a pulse with SC after entering a dispersive medium will come out with the bluer side of the pulse lagging behind its redder counterpart, due to the temporal dispersion induced by the medium. From this, PFT is calculated by the following equation:

$$PFT = PFT_{AD} + PFT_{SC+TC}[30,31] \quad (1)$$

where PFT_{AD} represents the PFT component due to AD and PFT_{SC+TC} represents the component due to SC and TC. If all couplings are present in the laser pulse, the spatio-temporal effects become complicated and hard to understand. It is also important to note that alongside PFT, there can be another manifestation of a spatio-temporal coupling known as wavefront rotation, *WFR*[31], which has been used experimentally for attosecond pulse generation[22,23], photonic streaking[32], pulse characterization and phase metrology.[33] It is then important to discern what spatio-temporal couplings are physically inherent in the beam to understand ultrafast laser induced phenomena.

3. Methods

Our experiments were carried out with a mode-locked regenerative amplified femtosecond laser system PHAROS (Light Conversion Ltd.) based on Yb:KGW lasing medium emitting a train of femtosecond pulses at 1030 nm with 200 kHz repetition rate. A set of grating compressors are used to induce TC and SC separately in order to have direct control on the PFT **(Figure 1)**. The first set is built into the laser set-up to compress or stretch the pulse duration by TC. By doing so, we increase/decrease the group delay dispersion *(GDD)* of the pulse accordingly. The second pulse compressor is used in a single pass geometry with a single grating and retro-reflector to induce SC, which is controlled by varying the distance between these two elements. The laser beam is then sent to a translation stage and focused into the bulk of fused silica with a 0.55 NA aspheric singlet lens or 1.4 NA oil immersion objective. The polarization state is controlled with a $\lambda/2$ waveplate to change the polarization orientation to be either parallel with the direction of SC (0°) or perpendicular to SC (90°).

In this experiment, the second grating compressor remains stationary over a fixed separation length. Thus, the SC is held constant at ~1 nm mm^{-1}. The amount of residual SC from the first grating set-up is ten times smaller in comparison to the amount of the frequency gradient from the second grating set-up. This alongside the compressor control for TC provides a complete method for control of spatio-temporal coupling in the laser pulses.

As substantial spatial chirp is added to the beam, it becomes elliptical. Thus, it is important to ensure that the spectral components of the beam are not clipped by the aperture of the focusing lens to reconstruct the initial bandwidth of the pulse correctly near the focus. To ensure this, a Galilean telescope is used to fit the elliptical beam into the back aperture of the focusing lens. As a result, the aperture of the lens is under filled reducing the effective numerical aperture. Considering this, all numerical apertures quoted in this publication are in their effective values.

In our experiment, angular dispersion is not present before the focusing lens when the SSTF set-up is in place, thus spatial and temporal chirp can be independently controlled. By measuring the slope of the wavelength vs. position using a fiber attached to a spectrometer we characterize the SC. The TC is controlled with the first compressor and is indirectly measured with an APE pulseCheck multi-shot autocorrelator. The GDD is then calculated by the following equation:

$$GDD = \frac{1}{4(\ln 2)} \sqrt{\left(\frac{c_B \Delta t_{out}}{\Delta v}\right)^2 - \left(\frac{c_B}{\Delta v}\right)^4} \quad (2)$$

where Δt_{out} is the measured pulse duration, Δv is the pulse bandwidth and c_B is a dimensionless constant depending on the pulse profile for the time-bandwidth product. The GDD value is confirmed by a second harmonic FROG and cross-checked with Kostenbauder matrix formalisms to ensure the experimental measurements match theoretical predictions.[34] With the measurements of TC and SC, the remaining PFT term in Equation 1 is calculated by multiplying the frequency gradient measured with the GDD of the characterized pulse yielding the PFT.

It is important to mention the focusing optics must also be taken into consideration as it may have a decisive effect on the overall PFT of the beam. Most objective lenses contain a considerable amount of glass, which can significantly increase the GDD of the pulse depending on the bandwidth of the pulse. This can drastically affect the PFT of the pulse and introduce other unwanted aberrations.[35] In our experiment, the bandwidth of our laser is relatively small (~ 8 nm); the effect of glass is negligible so all spatial-temporal couplings are controlled solely by the grating set-ups.

In our experimental conditions, we have two cases of spatio-temporal couplings. In the first case, the laser pulse is transform limited before the second grating set-up, which then stretches the pulse to ~4 ps. This increases the PFT at the focusing optics to 0.64 fs μm^{-1} (*With PFT*). In

the second case, the GDD induced by the second grating set-up is pre-compensated with the internal grating compressor in the laser, making PFT = 0 before the focusing lens (*No PFT*) so that the pulse remains transform limited with SC (~400 fs locally). The beam is then focused in a wide SSTF configuration, which yields a circularly symmetric focus despite ellipticity at the focusing lens caused by spatial chirp.[35]

4. Observations

To demonstrate the importance of the residual spatio-temporal couplings evident in typical ultrafast lasers, the beam emitted by the laser system was directly focused into the bulk of fused silica. Characterization of the spatio-temporal couplings in the beam emitted by our laser system clearly indicated that both AD and SC are present. In the horizontal direction of the beam, the SC is changing along propagation meaning AD is present. In the vertical direction, SC remains somewhat constant along propagation. At the focusing lens, $SC_x = 0.1$ nm mm^{-1} and $SC_y = 0.08$ nm mm^{-1}. This laser beam was focused with a NA = 0.55 lens and ten 300 fs, 0.5 μJ pulses were shot into the bulk with varying polarization with respect to the SC direction, resulting in void modification within the bulk **(Figure 2)**. Inspecting the cross-sections under an optical microscope, a clear difference was observed for the polarization parallel to SC (*0*°), where a long chain of voids stretching to the focus is seen, as opposed to the polarization perpendicular to SC (*90*°), where only a single void is seen at the top of the structure (Figure 2a). Also during the exposure, the white light emission was visibly brighter when polarization was perpendicular to the SC, confirming the observation made in the preliminary study.[25] The observed difference of structures is corroborated with experiments performed in fused silica with a typical titanium-sapphire laser (Coherent RegA 9000) (Figure 2b).

With respect to polarization multiplexed data storage[36], precise spot modification in the bulk of a transparent medium with tailored birefringence is necessary for the encoding of information. The laser-induced birefringence was characterized with the quantitative

birefringence measurement system (CRi Abrio; Olympus BX51). Focusing into the bulk of fused silica with NA = 0.75, a strong sinusoidal modulation in birefringence is observed with respect to the resulting slow-axis orientation of the structures **(Figure 3)**. The modulation is apparent for different pulse energies and shifts in polarization dependence when changing the repetition rate from 200 kHz to 500 kHz (Figure 3). This proves that spatio-temporal couplings that exist in typical ultrafast laser systems are extremely complex and can cause drastic effects on the overall modification induced in glass.

To determine what causes this polarization dependence in modification, the SSTF set-up was placed into the experimental design (Figure 1). The AD was removed in the horizontal direction with the second grating compressor and an additional SC was induced. A series of dots were then printed into the bulk of a fused silica sample with NA = 0.43 using the SSTF set-up. The qualitative analysis of the laser induced structures was performed by inspecting them under an Olympus BX51 optical microscope and with quantitative phase microscopy[37] (QPM). When varying the polarization state of the writing laser beam from 0° to 90° with respect to SC, a clear difference in the morphology of the structure was observed from the top and the cross-section **(Figure 4)**. When polarization is parallel to the direction of SC, the structures exhibit spherical symmetry with and without PFT. The modification is localized slightly above the focal region, being ~1 – 2 µm in diameter. When polarization is perpendicular (i.e. 90°) to the SC direction, the modification is observed to be stronger. Stress is induced along the direction of SC and the modified region is elongated in that direction to ~3-5 µm. From the cross-section, the laser-induced structure is larger and more dispersed in stark contrast to a circularly symmetric structure for 0°. The area around the structure shows a larger phase difference, due to the larger stress in the modification-induced region. The difference in modification for the two polarization states is observed within the bulk at various depths. However, when focusing on the surface of the fused silica, no observable difference is seen

between the orthogonal polarization states, confirming that the polarization dependence observed in modification is a nonlinear effect.

When investigating how the polarization dependence evolves within the first 10 pulses, it becomes clear that the effect increases with longer exposure **(Figure 5)**. No observable differences can be seen with the first pulse; however, the void modification becomes larger with subsequent pulses. The polarization dependence between orthogonal polarization states become more apparent after a few pulses, exhibiting elongation in void structure when polarization is perpendicular to SC and circularly symmetric voids when polarization is parallel. After 5-6 pulses, the elongation increases while the parallel polarization based structures remain circularly symmetric, further separating the modification induced by the two polarization states. The evolution in void structure emphasizes how the effect becomes stronger for longer exposure similar to what is observed in the bare beam case (Figure 2b).

When increasing the number of pulses overlapping in one spot even further, the void formation turns into a nanograting type of modification, revealed via birefringence formation [38] and with NA = 0.43, the difference between the orthogonal orientations becomes less apparent **(Figure 6)**. In both cases, the greatest difference in measured retardance is seen within the first 100 pulses with nanograting formation being initiated earlier when polarization is orthogonal to SC. But as the number of pulses increased past 100, the ratio of retardance between 90° and 0° drops from 0.6 - 0.8 to 0. The polarization dependence in modification is also less apparent at higher pulse energies for NA = 0.43, even though slight differences reside in the structure closer to the geometric focus. This indicates that the polarization dependence is dependent on the location where the nonlinear effects are initiated. Sufficient superposition of the spectral components is necessary to maximize the benefits seen by SSTF. Therefore, depending on the location of the nonlinear interaction or if focusing is not tight enough, the benefits of SSTF are minimized, as well as the polarization dependence (Figure 6).

In comparison to modification under conventional focusing conditions (CF), the transition to nanograting occurs much earlier. With SSTF, the transition occurs within the first tens of pulses whereas with CF, nanograting formation appears around 100 pulses for the equivalent pulse parameters of the two cases discussed. It should also be noted that the maximum retardance achieved within 100000 pulses in the *No PFT* case is roughly twice the retardance achieved under CF conditions. The ability to minimize the nonlinear interaction in the bulk with SSTF to a smaller volume near the focal plane provides an avenue to have stronger modification than what would be observed with CF, allowing one to attain stronger modification in a shorter period of exposure.

To check the hypothesis about the location of nonlinear interaction with respect to the polarization dependent modification, a series of structures were written with tighter focusing. When focusing into the bulk of fused silica using a NA = 0.9 oil immersion objective, the modification is localized closer to the focus and the more apparent manifestation of the polarization dependence is observed **(Figure 7)**. In this case, Type II modification is induced and a clear sinusoidal dependence is observed in the retardance of the structures with highest values measured for the polarization perpendicular to the direction of SC. The sinusoidal dependence is observed through a range of pulse densities but the ratio of the strength of retardance between 0° and 90° lowers from roughly 3:1 to 1.5:1 when increasing pulse density. This can be explained by a combination of thermal effects with the lateral growth of the structures, when regions further from the focus are modified.[39] These two factors will contribute to diminishing the effect of spatio-temporal couplings. Moreover, the shape of the structures is indicating a similar behaviour observed at weaker focusing conditions. The structures written with parallel polarization were circularly symmetric, whereas structures induced with perpendicular polarization were elongated in the SC direction.

5. Discussion

It is quite evident that spatio-temporal couplings play a significant role with respect to material modification. What is not well understood is how these couplings are altered by focusing. Recently, simulations and experiments have been developed to evaluate the effect optical aberrations would play in SSTF experiments[35], while others have shown how spatio-temporal couplings behave at the focus in air and in glass for particular situations[8,40,41], demonstrating how important these couplings are to the focusing propagation.

For the two cases discussed in this study, propagation simulations were conducted to demonstrate the evolution of spatio-temporal couplings when going from the lens to the focus. This sheds light on the origin of the anisotropy induced by polarization. The pulse before the lens has the following electric field distribution **(Figure 8)** [31]:

$$\vec{E}(x,y,t) = \vec{E}_0 \exp\left\{-\frac{x^2}{d_x^2} - \frac{y^2}{d_y^2} - 2pxct - \left(\frac{1}{\tau^2} - i\beta\right)t^2 - i\omega_0 t\right\} \quad (3)$$

where d_x^2 and d_y^2 are the beam widths along the x and y axes in the plane perpendicular to the beam propagation axis *z*, τ is the temporal width, β is the TC, ω_0 is the laser frequency and *p* is the space-time coupling term. It is a complex number with the real part representing the PFT and the imaginary part representing the WFR (or TVA).[31] Its value is controlled by the grating pair introduced between the laser and the focusing lens (Figure 1). Based on the two cases discussed in this publication, the induced SC is the same (Figure 8c) introducing ellipticity into the fluence distribution at the focusing lens with the aspect ratio a = 1.3 (Figure 8a) while AD is zero. However, the TC is different for both cases. In the first case (*With PFT*), the SC alongside the TC leads to PFT before the lens (Figure 8b) with a negligible WFR (Figure 8e). In contrast, in the second case (*No PFT*), SC is the same as the previous case but

with no TC present by the grating set-up effectively making PFT zero (Figure 8d) while introducing WFR (Figure 8f).

To understand what causes this polarization dependence, an identification of the major spatio-temporal coupling that is seen in and out of the focus is needed. However, a paraxial approximation in focusing assumes no polarization dependence. Therefore, to explain quantitatively how the coupling between polarization and spatio-temporal couplings in the focus operates, a non-paraxial analysis of the field structure near the focus is needed. When focusing a spatially chirped laser pulse with a high-NA lens[42,43], the spectral components propagate at angles relative to the original propagation direction, thus implying a dependence of the focusing conditions on the beam polarization and AD. The propagation of a converging laser beam is described by the wave equation for the envelope of the vector potential amplitude, $\vec{A} = \vec{A}(x, y, z, t')e^{(-i\omega_0 t + ik_0 z)}$:

$$2ik_0\partial_z\vec{A} + {\vec{\nabla}_\perp}^2\vec{A} = -{\partial_z}^2\vec{A} \tag{4}$$

where $t' = t - \frac{nz}{c}$ is the retarded time, n is the refractive index and $k_0 = n\omega_0/c$ is the laser wave number. In the paraxial approximation, the second derivative of the amplitude along the propagation direction is small and neglected. In this case, the electric field is defined by the time derivative of the potential $\vec{E} = i\omega_0\vec{A}$. Beyond the paraxial approximation, the right hand side of Equation 4 needs to be accounted for since it becomes of the order of NA^2.[44,45] Furthermore, a beam convergence leads to the appearance of the scalar potential, Φ, which arises from the Lorentz gauge $i\omega_0 n^2\Phi = c^2\nabla\cdot\vec{A}$ and maintains the zero divergence of the laser electric field. To calculate the non-paraxial corrections for an optical beam, techniques involving a circular cross-section have been developed.[44,45] We extended it to the case of an elliptical beam (Refer to Supporting Information).

The nonlinear effects observed during the experiment are defined by the local strength of the electric field. The nonlocal effects depend on the laser polarization with respect to the spatio-temporal couplings and thus introduce an anisotropy in the electric field distribution. Therefore, the fluence in the focal plane and the distribution along the propagation axis of the beam plays a vital role in the origin of the polarization dependence in modification. According to the experimental observations, the polarization dependence is a multi-pulse irradiation effect. This is in agreement with the theoretical analysis showing a very small polarization effect in the second order on the paraxial parameter, NA **(Figure 9)**. When compared against a case similar to the *No PFT* case but without spatio-temporal couplings (*no SC*; $\gamma = 0$) the SC leads to broadening of the focal spot in the chirp direction, thus producing an almost circular symmetric shape of the fluence (Figure 9a).

The laser characteristics in the focal plane for both cases are shown (Figure 9b-e). While the fluence distribution is the same, in both cases, the intensity distributions are quite different. Previous studies showed there is always a non-zero PFT at the focus when focusing a spatially chirped beam due to the AD induced by the lens [41,46], which is confirmed in our non-paraxial calculation. However, when focusing in glass, the PFT evolution in and out of the focus can be drastically different due to the initial state of the pulse at the lens. Inducing TC to the pulse drastically alters the evolution of PFT in and out of the focus. While PFT is observed in the first case at the lens, there is practically no PFT in the focal spot (Figure 9b, d) since the laser intensity is at a maximum in the spot center because of TC. Conversely, in the *No PFT* case, the PFT at the focus is evident (Figure 9c, e). Therefore, PFT may not be the origin of the observed effect as originally thought since the polarization dependence is observed in both cases, while their intensity distributions are drastically different. However, in both cases, SC remains the same. Focusing transforms the SC in the coordinate space into AD in the k-vector

space. We then conclude that this polarization dependence in modification originates from the angular dispersion upon tight focusing that derives from the initial spatial chirp.

It should be noted that non-paraxiality in itself affects the polarization contributions at the focus, introducing anisotropic effects in light-matter interactions.[47] Therefore, the electric field contributions at the focus need to be taken into consideration (**Figure 10, Figure 11**). The transverse electric field components at the focus for both *With PFT* and *No PFT* cases are very similar to the laser intensity distributions observed at the focus (Figure 9b-e). In opposite, the axial component for both *With PFT* (Figure 10a, c) and *No PFT* (Figure 11a, c) are quite different. However, the axial components contribute about 2% to the overall electric field at the focus (Figure 10b, d, Figure 11b, d). While anisotropic effects from the non-paraxial focusing are indeed present, the anisotropic and non-paraxial terms are relatively small making them difficult to observe in single-pulse irradiation. The contribution could be quite important with further irradiation of 100 or more pulses but would not become noticeable within the first few pulses. Therefore, the anisotropic photosensitivity observed in this study between the parallel and perpendicular polarizations is primarily due to the AD.

Interestingly, the observed damage is anisotropic (Figure 5) even though the fluence shape in the focus is round (Figure 9a). At the moment, there is no complete explanation for this fact. In experiment, we observe that the phenomenon occurs after multiple pulses. The effect of the subsequent pulse scattering on the material modifications induced by the previous pulse could be an origin of this effect. The scattering takes place in the plane perpendicular to the laser polarization and may lead to spreading modification in that plane. However, the multi-pulse simulations accounting for material modification effects are extremely difficult to model because of complicated physics intervening the non-paraxial propagation and sub-wavelength material inhomogeneities in the focal zone alongside the incubation effects. Once some macroscopic modification is induced, it behaves as a scattering center for further pulse

irradiation. The difference in structure for the orthogonal polarization states can scatter the incoming light differently, altering the modification for longer irradiation and change the distribution of the modification. The contrast in modification between the orthogonal polarization states would then increase with longer exposure. With the initial modification after the first pulse, the observed anisotropic behavior would emerge with further pulse irradiation. The concept of the initial pulse developing a "seed" in the glass, which eventually introduces polarization dependences for further pulse irradiation have been discussed before.[48,49] But these studies do not involve spatio-temporal couplings or non-paraxial effects. A multi-pulse model is currently under development to see how the polarization coupling with SC evolves with further pulse irradiation.

Ensuring that AD before the lens is zero and that the Wide-SSTF geometry used in the experiment leads to a circularly symmetric focus[35], the only spatio-temporal coupling that can cause the observed polarization dependence is the induced SC. It becomes apparent that when using typical ultrafast laser systems with chirp amplification set-ups, the polarization dependence will be present, affecting the material nanostructuring. In some cases, the polarization dependence in modification can be minimized by overlapping adjacent tracks.[27] However, this is not always possible and for applications like waveguide manufacturing and polarization multiplexed data storage, the polarization dependence plays a major role. This motivates a discussion of how to deal with this issue when modifying glass in a singular position. One possibility is to add a dynamic compensation mechanism, such as using a spatial light modulator *(SLM).*[29] This inherently is difficult for many reasons. One is power limitations due to the damage threshold of typical SLMs. Another is the difficulty in producing holograms on the SLM to compensate for the spatio-temporal couplings across the entire beam spot of the laser pulse. This can be overcome by using traditional dispersive element techniques like grating or prism compressors. However, depending on the quantity and type of

spatio-temporal coupling inherent in the laser beam, large propagation distances may be needed which can be detrimental to the beam spot and overall beam quality factor. One also needs to take into consideration the correction of aberrations from the focusing optics especially when working with lasers of higher bandwidths.

Instead of correcting for the polarization dependence in modification, one might harness it for an extra degree of control for modification. Once understanding what spatio-temporal couplings lie within the laser beam being used and how they behave in modification, utilization of the polarization dependence allows tailoring of the relative strength of the modification. Depending on the application, different polarization orientations with respect to the SC will appear more beneficial. For overall larger retardance and stronger modification outside of the focal plane, polarization should be oriented perpendicular to the SC direction. This is highlighted by the observation of stronger white light emission during laser exposure. Yet in this regime, the modification is elongated along the chirp direction, which could hinder applications where symmetrical modification is needed. On the other side, symmetrical modification is attained by setting the polarization to be parallel to the SC. In this regime, the modification reaches closer to the focal plane but is observably weaker than the orthogonal case, with longer exposures needed to reach the same modification thresholds. By simply rotating the polarization state with respect to the orientation of SC, the relative strength of modification in a spot can be controlled potentially reducing the manufacturing time for larger scale applications. Another method to use alongside the spatio-temporal couplings is to rotate the spatio-temporal couplings with rotational optics, such as a dove prism[50], with the polarization to ensure modification is symmetric and of the same strength.

A balance between SC and the effective NA of the focusing optic needs to be determined depending on the laser source used in order to ensure tight focusing for the effect to be dominant. Moreover, it is clear that SSTF is beneficial in inducing stronger modification under

shorter irradiation times (Figure 6). Simply by adding SC to the beam, the nonlinear interaction is localized closer to the focal plane as opposed to CF, similar to what has been discussed in previous studies.[7,9,12] Providing an avenue to attain stronger modification with up to 10x less the amount of pulses can again potentially reduce the manufacturing time for larger scale applications or improve the writing speed associated with polarization multiplexed data storage.

6. Conclusion

Spatio-temporal couplings play a pivotal role in the dynamics of ultrafast laser material modification. They are present in all ultrafast laser systems and cause unpredictable results in laser nanostructuring. To alleviate this issue, we have successfully untangled spatial and temporal chirp with the use of grating compressors and illustrated an additional level of control on the strength of modification. In doing so, a polarization dependence in modification is observed in fused silica after multi-pulse exposure, making it an inherent physical phenomenon in ultrafast light-matter interaction. This effect arises from angular dispersion in the focus that originates from a frequency gradient in the laser pulse and not pulse front tilt as originally thought. Modification can be tailored by changing the polarization state of the laser pulse with respect to the direction of spatial chirp. The modification is also stronger under these conditions in comparison to conventional focusing, providing an avenue to attain stronger modification in a smaller volume with shorter pulse irradiation times. This effect is a non-paraxial, multi-pulse phenomenon, becoming more apparent for tighter focusing regimes and longer exposures when the modification takes place close to the focal plane. While currently there is no full explanation behind the mechanism of the phenomenon, it is potentially due to the observed axial component of the electric field alongside the interaction with the modification that takes place in the first pulse. As SSTF becomes more attractive in ultrafast laser nanostructuring, the ability to control the strength of modification with the polarization state can benefit not only tailoring the

strength of modification but also the manufacturing time for time consuming based applications to deliver stronger modification in a shorter time.

Acknowledgements. The authors would like to acknowledge fruitful discussion with Dr. Martynas Beresna during the initial stages of this work. This work was funded by the Engineering and Physical Sciences Research Council (EPSRC Project No. EP/M029042/1). All data in this paper was deposited into the University of Southampton Library Repository (doi:10.5258/SOTON/D0008)

Keywords: (Spatio-Temporal Coupling, Ultrafast Phenomena, Laser Material Processing)

References

1. Gessner, O., Lee, A.M.D., Shaffer, J.P., et al. (2006) Femtosecond multidimensional imaging of a molecular dissociation. *Science*, **311** (5758), 219–222.
2. Brixner, T., Damrauer, N.H., Niklaus, P., and Gerber, G. (2001) Photoselective adaptive femtosecond quantum control in the liquid phase. *Nature*, **414** (6859), 57–60.
3. Zipfel, W.R., Williams, R.M., and Webb, W.W. (2003) Nonlinear magic: multiphoton microscopy in the biosciences. *Nat. Biotechnol.*, **21** (11), 1369–1377.
4. Chung, S.H., and Mazur, E. (2009) Surgical applications of femtosecond lasers. *J. Biophotonics*, **2** (10), 557–572.
5. Strickland, D., and Mourou, G. (1985) Compression of amplified chirped optical pulses. *Opt. Commun.*, **55** (6), 447–449.
6. Perry, M.D., and Mourou, G. (1994) Terawatt to petawatt subpicosecond lasers. *Science*, **264** (5161), 917–924.
7. He, F., Xu, H., Cheng, Y., et al. (2010) Fabrication of microfluidic channels with a circular cross section using spatiotemporally focused femtosecond laser pulses. *Opt. Lett.*, **35** (7), 1106–1108.
8. He, F., Wang, Z., Zeng, B., et al. (2014) Three-dimensional patterning in transparent materials with spatiotemporally focused femtosecond laser pulses. *Optoelectron. Imaging Multimed. Technol. III*, **9273**, 927316.
9. Kammel, R., Ackermann, R., Thomas, J., et al. (2014) Enhancing precision in fs-laser material processing by simultaneous spatial and temporal focusing. *Light Sci. Appl.*, **3** (5), e169.
10. Durfee, C.G., and Squier, J.A. (2015) Breakthroughs in photonics 2014: Spatiotemporal focusing: Advances and applications. *IEEE Photonics J.*, **7** (3), 1–6.
11. Thomas, J.U., Block, E., Greco, M., et al. (2014) Simultaneously spatially and temporally focusing light for tailored ultrafast micro-machining. *Spie Lase*, **8972**, 897219.
12. Kammel, R., Bergner, K., Thomas, J.U., et al. (2016) Simultaneous spatial and temporal focusing: A route towards confined nonlinear materials processing. *Proc. SPIE*, **9736** (Laser-based Micro-and Nanoprocessing X), 1–10.
13. Katz, O., Bromberg, Y., Small, E., and Silberberg, Y. (2010) Focusing and Compression of Ultrashort Pulses through Scattering Media. *Nat. Photonics*, **5** (May), 1–6.
14. Durst, M.E., Zhu, G., and Xu, C. (2006) Simultaneous spatial and temporal focusing for axial scanning. *Opt. Express*, **14** (25), 12243–54.
15. Durst, M.E., Zhu, G., and Xu, C. (2008) Simultaneous spatial and temporal focusing in nonlinear microscopy. *Opt. Commun.*, **281** (7), 1796–1805.
16. Block, E., Greco, M., Vitek, D., et al. (2013) Simultaneous spatial and temporal focusing for tissue ablation. *Biomed. Opt. Express*, **4** (6), 831–41.
17. McCabe, D.J., Tajalli, A., Austin, D.R., et al. (2011) Spatio-temporal focusing of an ultrafast pulse through a multiply scattering medium. *Nat. Commun.*, **2** (May), 447.
18. Gu, X., Akturk, S., and Trebino, R. (2004) Spatial chirp in ultrafast optics. *Opt.*

Commun., **242** (4–6), 599–604.

19. Gabolde, P., Lee, D., Akturk, S., and Trebino, R. (2007) Describing first-order spatio-temporal distortions in ultrashort pulses using normalized parameters. *Opt. Express*, **15** (1), 242–51.
20. Bor, Z., Racz, B., Szabo, G., et al. (1993) Femtosecond pulse front tilt caused by angular dispersion. *Opt. Eng.*, **32** (10), 2501–2504.
21. Torres, J.P., Hendrych, M., and Valencia, A. (2010) Angular dispersion: an enabling tool in nonlinear and quantum optics. *Adv. Opt. Photonics*, **2** (3), 319.
22. Wheeler, J.A., Borot, A., Monchocé, S., et al. (2012) Attosecond lighthouses from plasma mirrors. *Nat. Photonics*, **6** (December), 829–833.
23. Vincenti, H., and Quéré, F. (2012) Attosecond lighthouses: How to use spatiotemporally coupled light fields to generate isolated attosecond pulses. *Phys. Rev. Lett.*, **108** (11), 1–5.
24. Trebino, R., Bowlan, P., Gabolde, P., et al. (2009) Simple devices for measuring complex ultrashort pulses. *Laser Photonics Rev.*, **3** (3), 314–332.
25. Kazansky, P.G., Shimotsuma, Y., Sakakura, M., et al. (2011) Photosensitivity control of an isotropic medium through polarization of light pulses with tilted intensity front. *Opt. Express*, **19** (21), 20657–64.
26. Kazansky, P.G., Yang, W., Bricchi, E., et al. (2007) "Quill" writing with ultrashort light pulses in transparent materials. *Appl. Phys. Lett.*, **90** (15), 151120.
27. Gecevičius, M., Beresna, M., Zhang, J., et al. (2013) Extraordinary anisotropy of ultrafast laser writing in glass. *Opt. Express*, **21** (4), 3959–68.
28. Vitek, D.N., Block, E., Bellouard, Y., et al. (2010) Spatio-temporally focused femtosecond laser pulses for nonreciprocal writing in optically transparent materials. *Opt. Express*, **18** (24), 24673–24678.
29. Salter, P.S., and Booth, M.J. (2012) Dynamic control of directional asymmetry observed in ultrafast laser direct writing. *Appl. Phys. Lett.*, **101** (14), 141109.
30. Akturk, S., Gu, X., Zeek, E., and Trebino, R. (2004) Pulse-front tilt caused by spatial and temporal chirp. *Opt. Express*, **12** (19), 4399–410.
31. Akturk, S., Gu, X., Gabolde, P., and Trebino, R. (2005) The general theory of first-order spatio-temporal distortions of Gaussian pulses and beams. *Opt. Express*, **13** (21), 8642–61.
32. Kim, K.T., Zhang, C., Ruchon, T., et al. (2013) Photonic streaking of attosecond pulse trains. *Nat. Photonics*, **7** (8), 651–656.
33. Quéré, F., Vincenti, H., Borot, A., et al. (2014) Applications of ultrafast wavefront rotation in highly nonlinear optics. *J. Phys. B At. Mol. Opt. Phys.*, **47** (12), 124004.
34. Kostenbauder, A.G. (1990) Ray-Pulse Matrices: A Rational Treatment for Dispersive Optical Systems. *IEEE J. Quantum Electron.*, **26** (6), 1148–1157.
35. Sun, B., Salter, P.S., and Booth, M.J. (2014) Effects of aberrations in spatiotemporal focusing of ultrashort laser pulses. *J. Opt. Soc. Am. A. Opt. Image Sci. Vis.*, **31** (4), 765–72.
36. Zhang, J., Gecevičius, M., Beresna, M., and Kazansky, P.G. (2014) Seemingly unlimited lifetime data storage in nanostructured glass. *Phys. Rev. Lett.*, **112** (3), 1–5.

37. Barty, A., Nugent, K.A., Paganin, D., and Roberts, A. (1998) Quantitative optical phase microscopy. *Opt. Lett.*, **23** (11), 817–819.

38. Mishchik, K., D'Amico, C., Velpula, P.K., et al. (2013) Ultrafast laser induced electronic and structural modifications in bulk fused silica. *J. Appl. Phys.*, **114** (13).

39. Shimotsuma, Y., Sakakura, M., Kazansky, P.G., et al. (2010) Ultrafast manipulation of self-assembled form birefringence in glass. *Adv. Mater.*, **22** (36), 4039–43.

40. He, F., Zeng, B., Chu, W., et al. (2014) Characterization and control of peak intensity distribution at the focus of a spatiotemporally focused femtosecond laser beam. *Opt. Express*, **22** (8), 9734–48.

41. Zhang, S., Wyrowski, F., Kammel, R., et al. (2014) Analysis of Pulse Front Tilt in Simultaneous Spatial and Temporal Focusing. *JOSA A*, **9135** (11), 2437–2446.

42. Born, M., and Wolf, E. (1980) *Principles of optics*, Pergammon Press Ltd., Oxford.

43. Wormell, P.M.J.. (2000) Advanced optical imaging theory. *Opt. Lasers Eng.*, **33** (3), 237–238.

44. Davis, L.W. (1979) Theory of electromagnetic beams. *Phys. Rev. A*, **19** (3), 1177–1179.

45. Salamin, Y.I. (2007) Fields of a Gaussian beam beyond the paraxial approximation. *Appl. Phys. B Lasers Opt.*, **86** (2), 319–326.

46. Durfee, C.G., Greco, M., Block, E., et al. (2012) Intuitive analysis of space-time focusing with double-ABCD calculation. *Opt. Express*, **20** (13), 14244–59.

47. Rekstyte, S., Jonavicius, T., Gailevicius, D., et al. (2016) Nanoscale Precision of 3D Polymerization via Polarization Control. *Adv. Opt. Mater.*, **4** (8), 1209–1214.

48. Zhang, J., Drevinskas, R., Beresna, M., and Kazansky, P.G. (2015) Polarization sensitive anisotropic structuring of silicon by ultrashort light pulses. *Appl. Phys. Lett.*, **41114**, 2–6.

49. Rudenko, A., Colombier, J., and Itina, T.E. (2016) From random inhomogeneities to periodic nanostructures induced in bulk silica by ultrashort laser. *Phys. Rev. B*, **75427**, 1–13.

50. Moreno, I. (2004) Jones matrix for image-rotation prisms. *Appl. Opt.*, **43** (17), 3373–81.

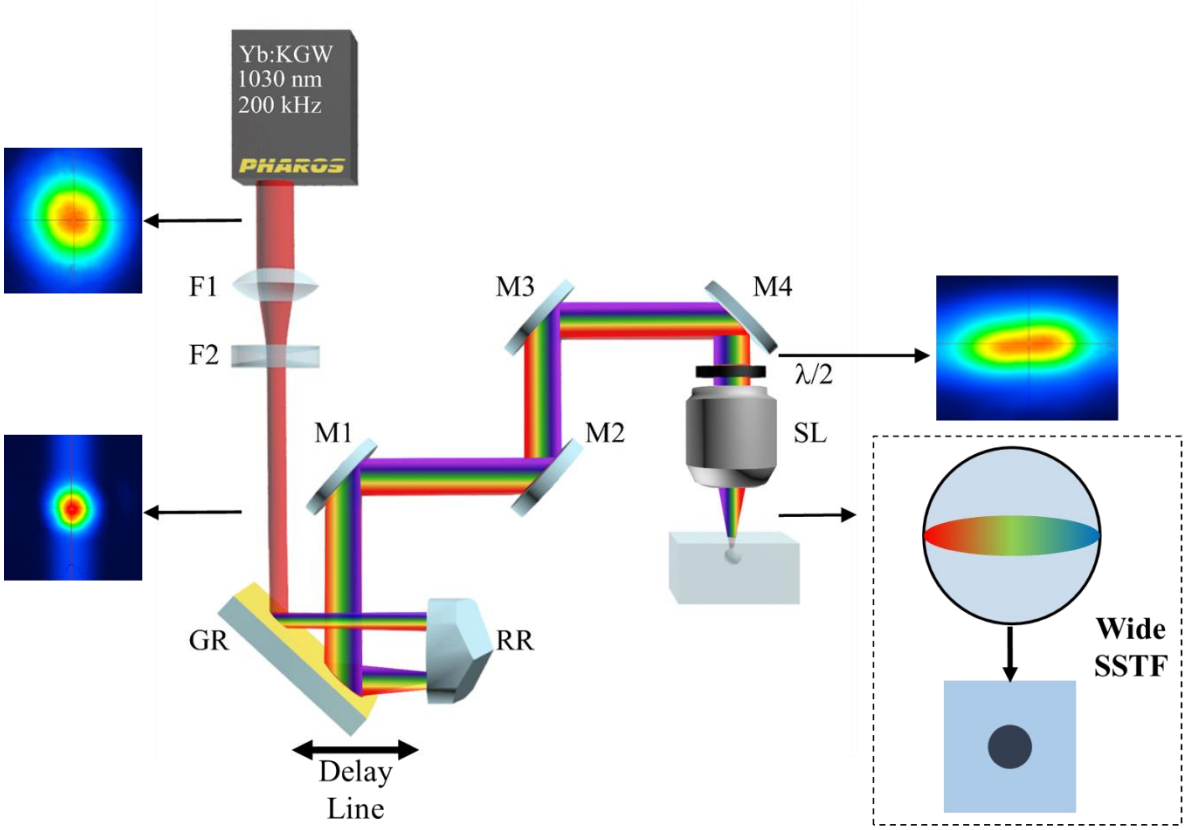

Figure 1. Double Grating Set-up for Full Spatio-Temporal Control. The first diffraction grating is integrated in the laser system and controls TC. The second grating in combination with a retroreflector enables tailoring of SC by simply varying the distance between these elements. A Galilean telescope ensures that the laser beam is not clipped by the rear aperture of the focusing lens. The addition of SC introduces ellipticity into the laser beam. However, a wide SSTF focusing geometry ensures that the beam spot near the focus, where light-matter interaction takes place, is circularly symmetric. (F1 = 200 mm, F2 = -100 mm, GR = Grating, RR = Retroreflector, M1-4 = Mirrors, λ/2 = Half-Waveplate, SL = Focusing lens).

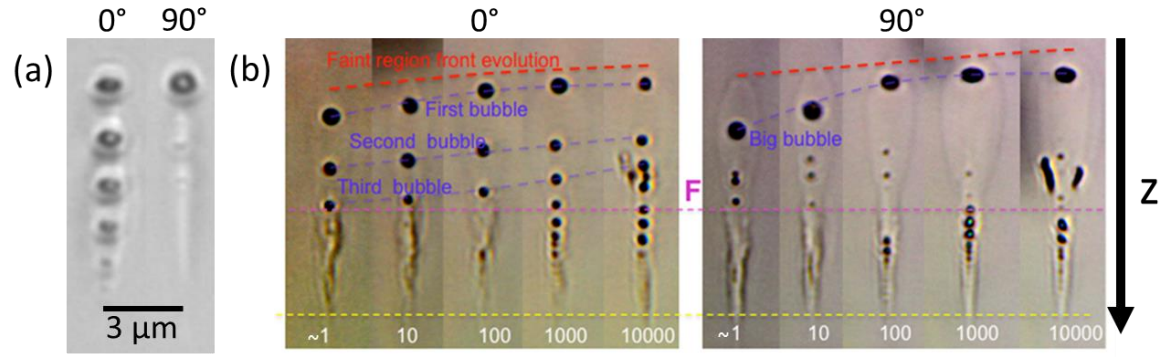

Figure 2. Optical Images of Fused Silica Regions Modified by Transform Limited Ultrafast Pulses (a) 10 pulses, E_p = 0.5 µJ, NA= 0.55, τ_p = 300 fs, f = 200 kHz, λ = 1030 nm; (b) E_p = 2.4 µJ, NA = 0.65, τ_p = 70 fs, f = 250 kHz, λ = 800 nm. When polarization is parallel to SC (0°), long chains of nano-voids are observed across the structure. Whereas, for perpendicular arrangement, only a single, enlarged void is seen at the top of the structure. The propagation direction of the laser, *z*, is indicated by the black arrow.

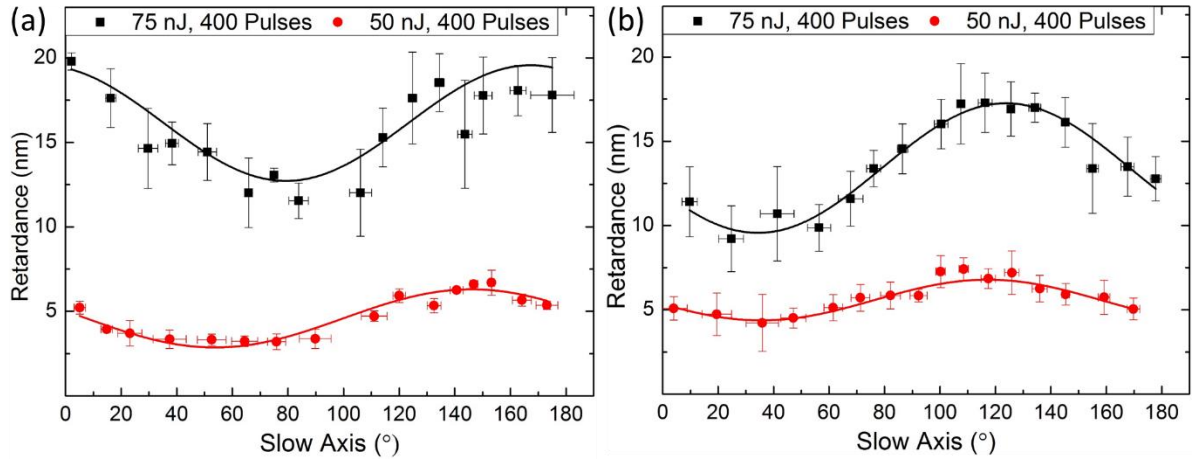

Figure 3. Retardance Measurements of Fused Silica Regions Modified by Tightly Focused (NA = 0.75) Femtosecond Pulses with Varying Polarization and Pulse Energy. (a) f = 200 kHz and (b) f = 500 kHz. The retardance value exhibits a sinusoidal modulation when varying the azimuth of the polarization plane. This modulation shifts when changing repetition rate making it difficult to understand the origin of the modulation and control strength of birefringence for digital information encoding.

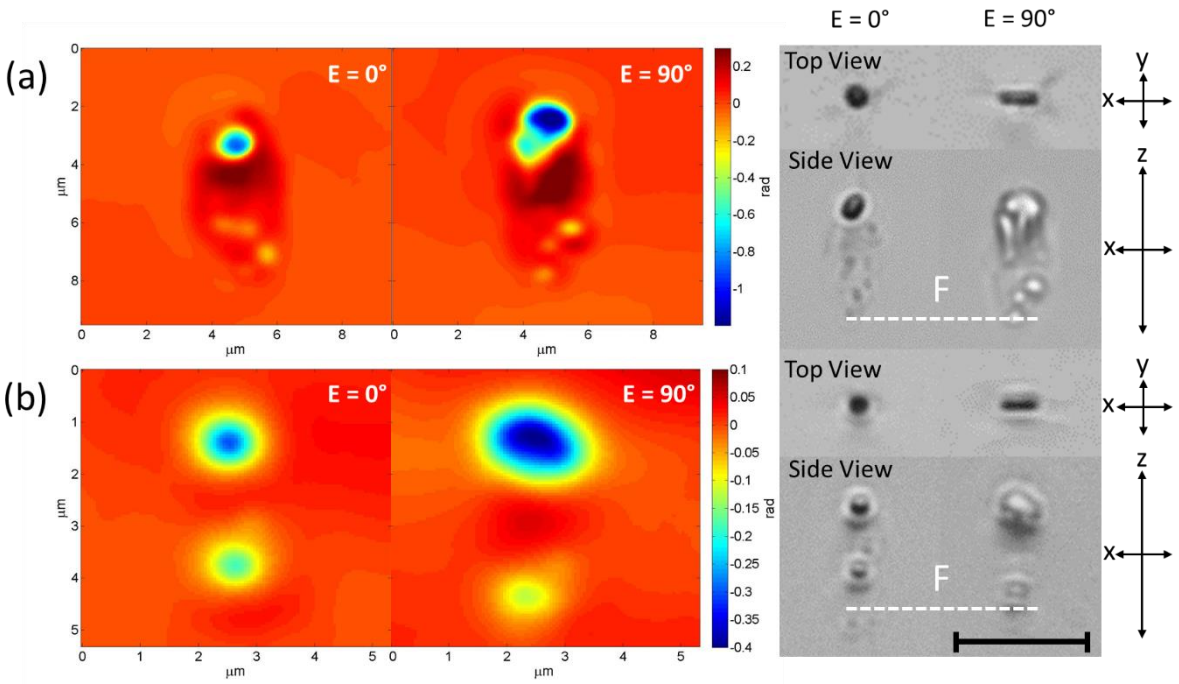

Figure 4. Optical and Phase Contrast Images of Modified Region after Irradiation with 10 Pulses. (a) With PFT, E_p = 0.5 μJ, NA = 0.43 and (b) No PFT, E_p = 0.35 μJ, NA = 0.43. Clear difference is observed when polarization rotates from parallel to SC (E = 0^0) to perpendicular to SC (E = 90^0). The cross-section of the structure is circularly symmetric if E = 0°. However, if E = 90^0, it becomes strongly elongated. The modification is more dispersed and exhibits larger phase variation when E = 90^0, indicating stronger structural change. The white dashed line in the optical images indicates the geometrical focal point. The scale bar is 4 μm.

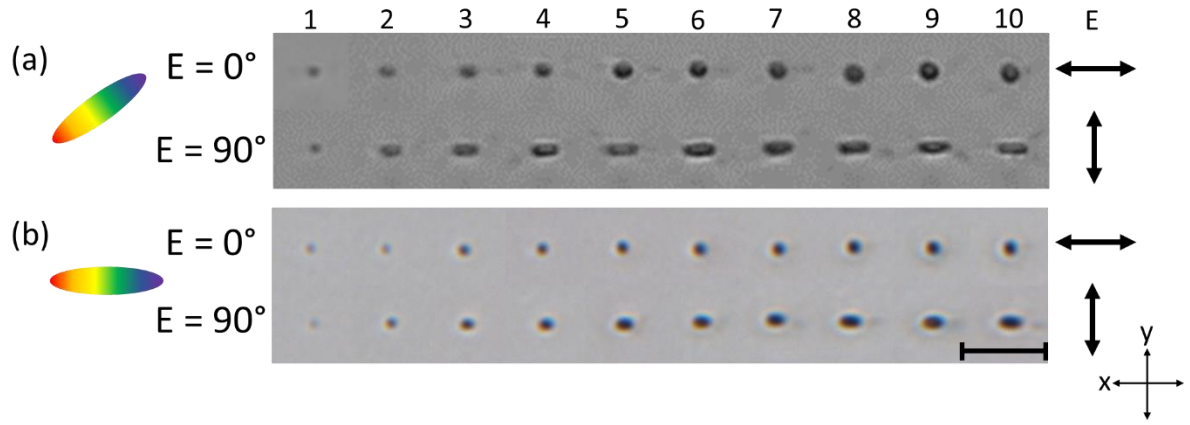

Figure 5. Evolution of Polarization Dependence over First 10 Pulses, Top View. Pulse energy 0.5 µJ, NA = 0.43 (a) With PFT and (b) No PFT. After the first pulse, the modification for the two polarization states are identical. Upon further pulse irradiation, the differences between the two polarization states emerge showing circularly symmetric structures when the polarization is parallel to the SC (E = 0°) and elongated along the SC direction when perpendicular to the SC (E = 90°). The difference continues to increase and becomes stronger with longer irradiation. Polarization is oriented as depicted by the black arrows. The scale bar is 5 µm. The PFT state before the lens is schematically shown for both cases.

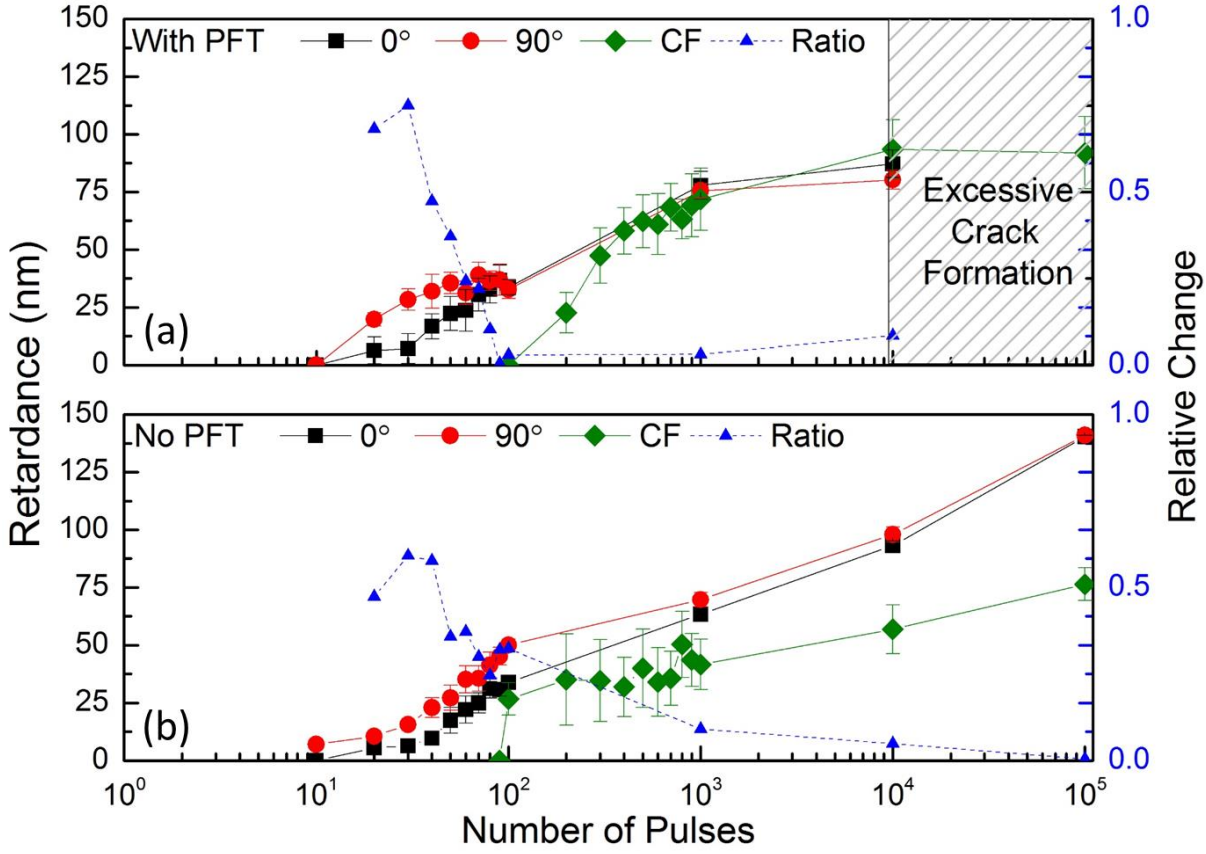

Figure 6. Retardance of Regions Modified with Femtosecond Pulses Focused with NA = 0.43 as a Function of Pulse Density. (a) With PFT, E_p = 0.5 μJ (b) No PFT, E_p = 0.35 μJ. Within the first 100 pulses, the structures printed with polarization orthogonal to SC (red circles) have larger retardance than those parallel (black squares). The relative change measured between 90° and 0° (blue triangles, $|Ret(90^0) - Ret(0^0)|/Ret(90^0)$) is 0.6-0.8 within the first 30 pulses and then begins to drop to zero as the pulse density increases. For the two cases discussed, the transition to nanograting occurs within the first tens of pulses whereas in equivalent conditions under conventional focusing (CF, green diamonds) the transition does not occur until after 10^2 pulses. The retardance achieved under SSTF conditions is larger, especially in the No PFT case where the total retardance after 10^5 pulses is roughly twice that achieved under CF, providing an avenue to attain stronger modification in a smaller focal volume under shorter irradiation times.

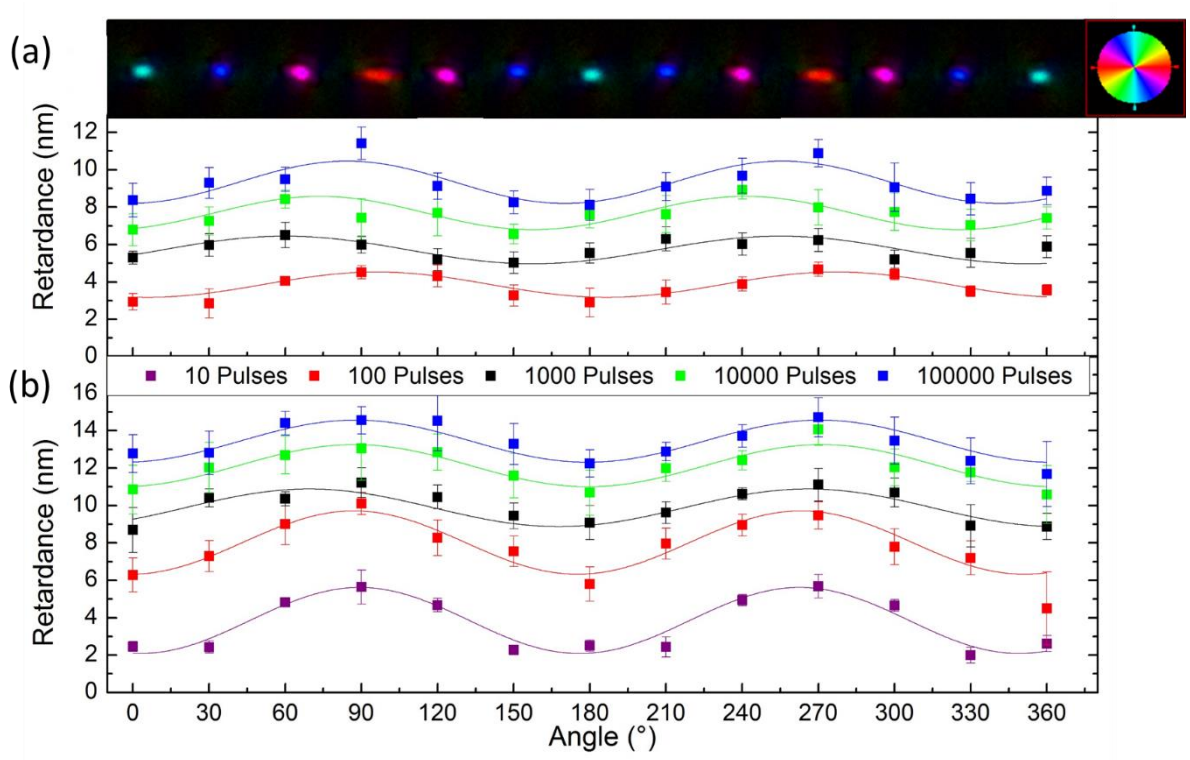

Figure 7. Retardance of Regions Modified with 100 nJ Femtosecond Pulses as a Function of Exposure Time and Polarization. (a) With PFT and (b) No PFT. Sinusoidal dependence of retardance is observed for perpendicular polarization yielding strongest birefringence. Ratio of birefringence strength diminishes with larger exposure times as a result of thermal effects but modulation in retardance is still evident. Structures (inset in figure) are circularly symmetric for 0^0 (light blue structure) and elliptically elongated for 90° (red structure) similarly to what is observed in NA = 0.43 case. The color of the structures represents the slow axis orientation, illustrated by the inset color wheel.

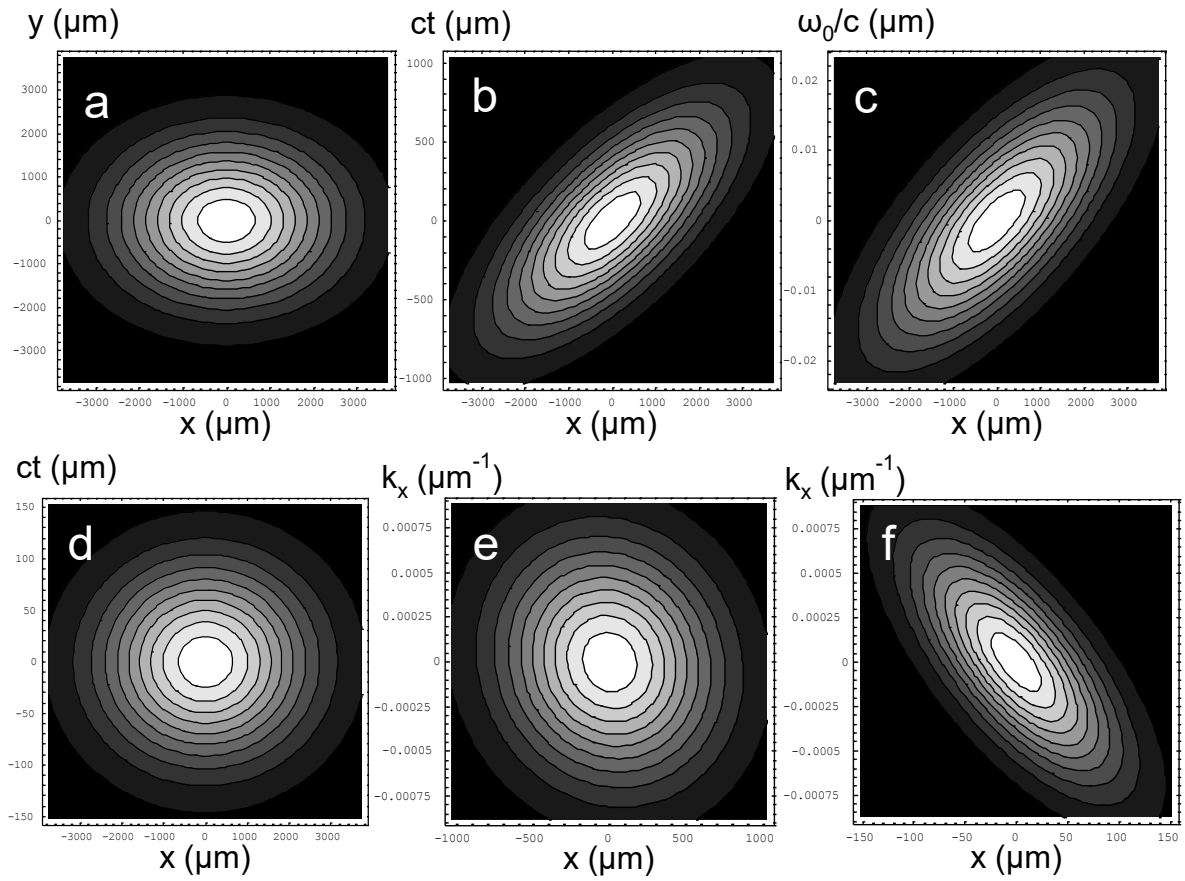

Figure 8. **Distribution of the Laser Beam at the Lens for the Two Cases Conducted in Experiment.** (a) Laser beam fluence for both cases at the lens. (b, d) The laser beam intensity distribution in the plane y = 0 for the cases (With PFT) and (No PFT), respectively. (c) The frequency distribution across the laser beam for both cases (i.e. SC). (e, f) The WFR of the beam at the lens in the plane y = 0 for the cases (With PFT) and (No PFT), respectively.

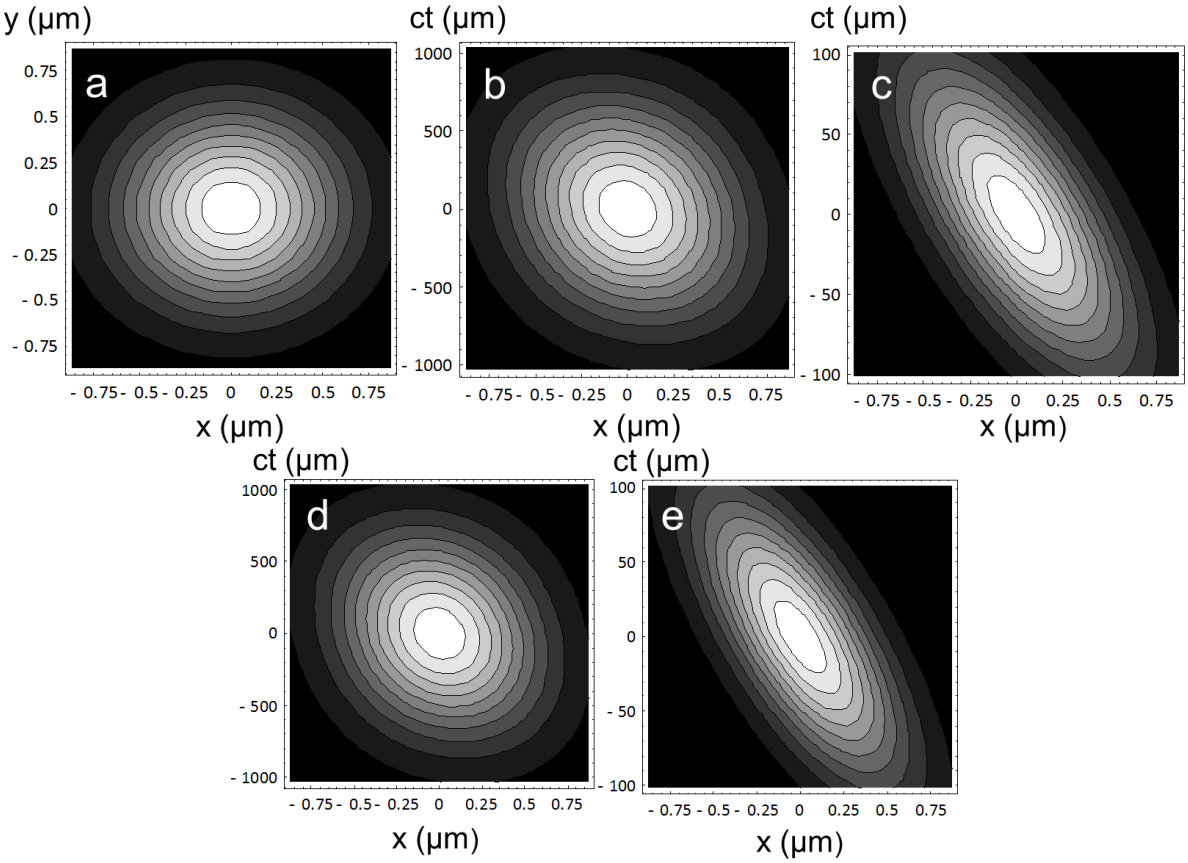

Figure 9. Distribution of the Laser Fluence (a) and Laser Intensity (b-e) in the Focal Plane z = F for polarization 0° (b, c) and 90° (d, e). (b, d) With PFT, (c, e) No PFT. The fluence distribution is the same in both cases regardless of the polarization state. When looking in the focal plane, the PFT observed is opposite of what is observed before the lens for both cases even with non-paraxial corrections. This furthers the conclusion that PFT is not the origin of the polarization dependence, as originally theorized, and that the polarization dependence is a multi-pulse phenomenon as observed in experiment.

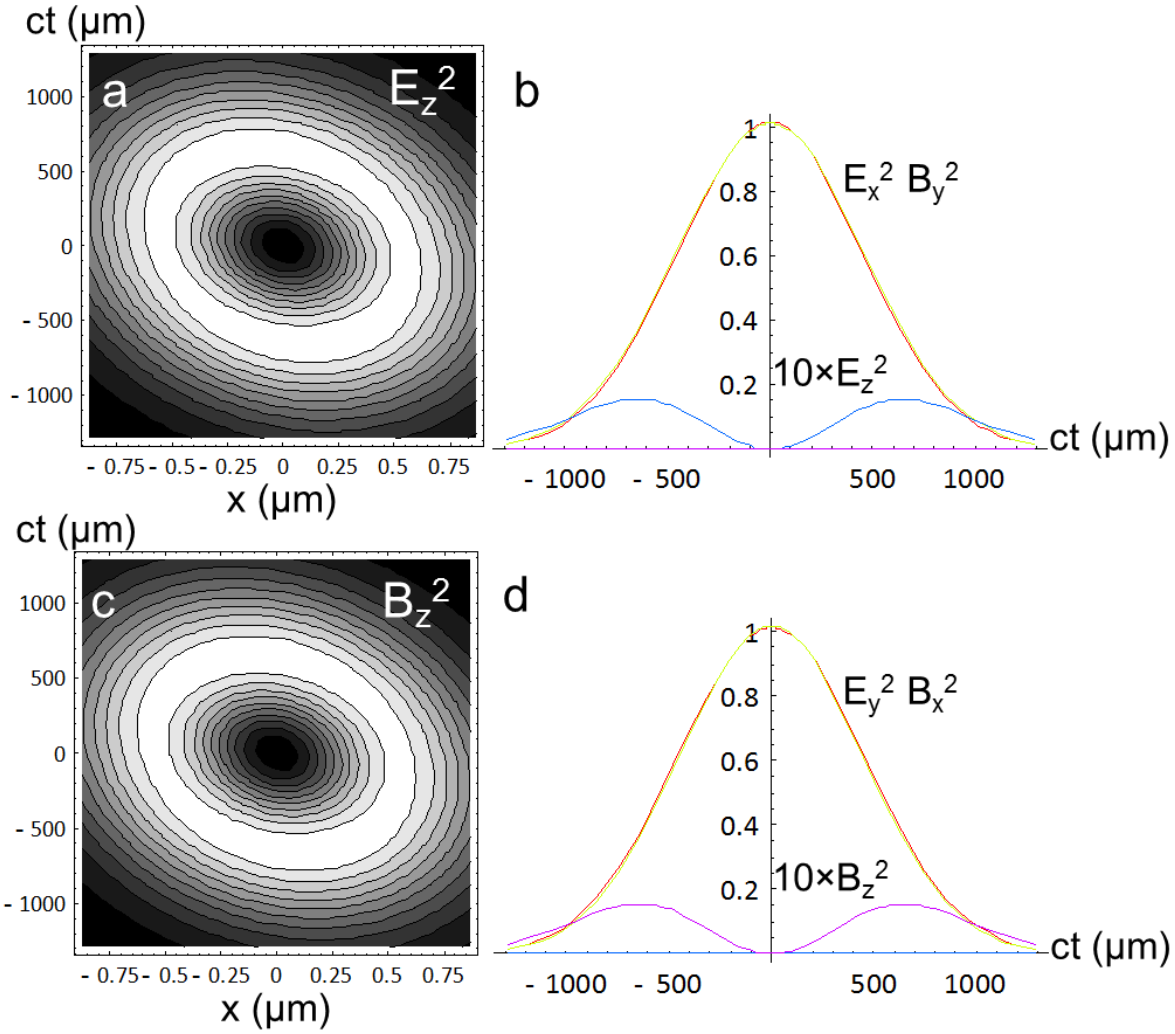

Figure 10. Axial Electric Field Contribution for the With PFT case at the focus z = F for polarization 0° (a, b) and 90° (c, d). (b, d) Relative amplitudes of components as a function of time. While the axial contribution is evident and different from its transverse counterparts, it results in roughly 2% of the overall electric field at the focus.

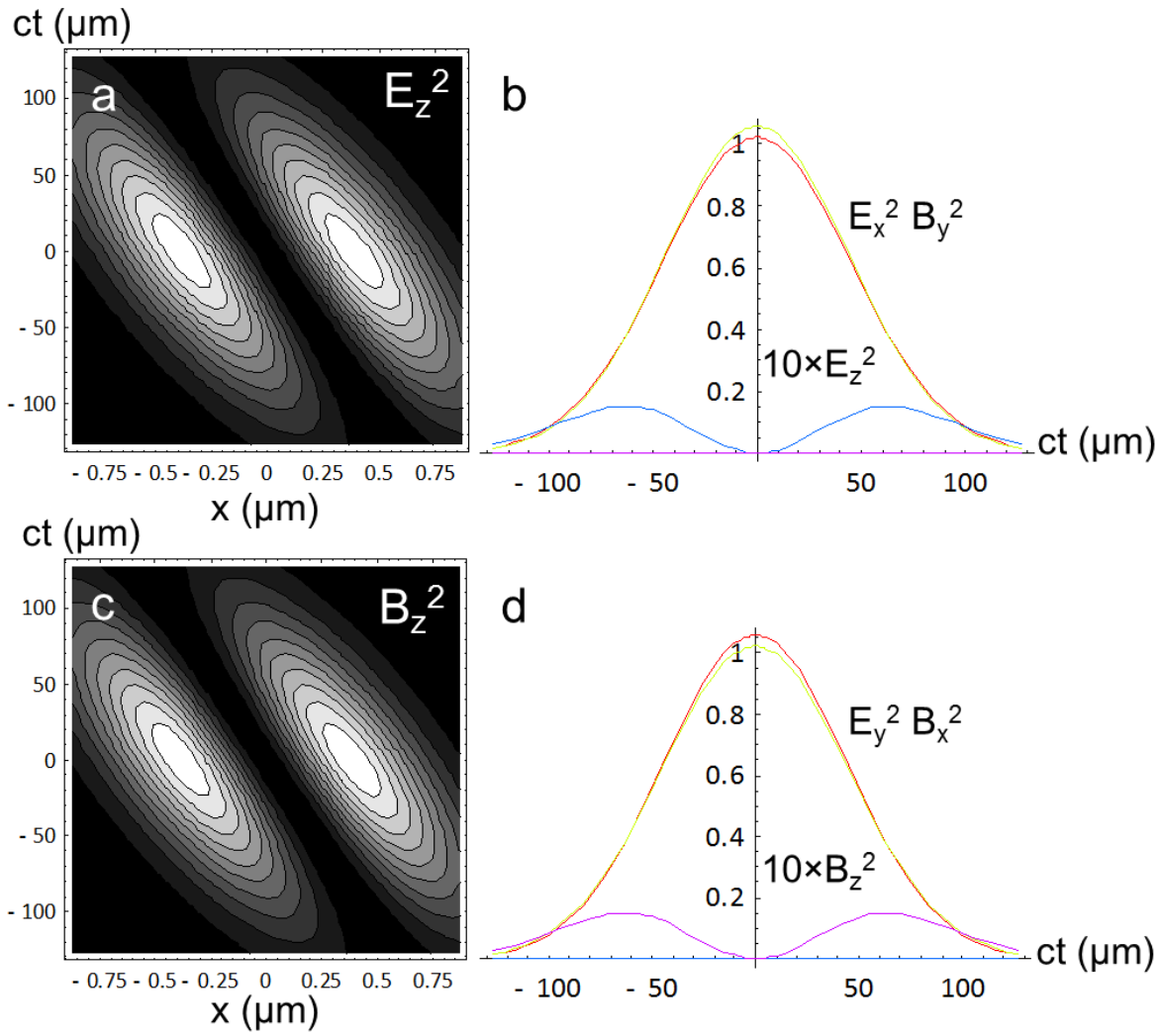

Figure 11. **Axial Electric Field Contribution for the No PFT case at the focus z = F for polarization 0° (a, b) and 90° (c, d).** (b, d) Relative amplitudes of components as a function of time. While the axial contribution is evident and different from its transverse counterparts, it results in roughly 2% of the overall electric field at the focus.

Contents